SECTIONAL AERODYNAMIC FORCES AND THEIR LONGITUDINAL CORRELATION ON A VIBRATING 5:1 RECTANGULAR CYLINDER

Francesco Ricciardelli[*], Antonino M. Marra[†]

[*]DIMET
University of Reggio Calabria, Via Graziella, Feo di Vito, 89060 Reggio Calabria, Italy
e-mail: `friccia@unirc.it`

[†] Department of Civil and Environmental Engineering
University of Florence, Via Santa Marta 3, 50139 Firenze, Italy
e-mail: `antonino.marra@dicea.unifi.it`

Keywords: Rectangular Cylinders, Wind Tunnel Testing, Aerodynamic pressures, Aerodynamic Forces, Correlation, Self-Excited forces.

Abstract. *The aerodynamics of simple geometries such as the circle, the square and the rectangle is of interest for both fundamental research and practical applications in many areas of Engineering. In particular, rectangular cylinders have received large attention due to the fact that they offer a broad range of types of aerodynamic and aeroelastic behaviour, depending on the aspect ratio. A wide variety of results of wind tunnel measurements and of CFD analyses are available in the literature. In this paper some features of the aerodynamics of a 5:1 rectangular cylinder are presented, as obtained from wind tunnel pressure measurements, through comparison between the case in which the cylinder is located in a smooth flow and the case in which it is located in a turbulent flow. In addition, in the case of an oncoming smooth flow, the aerodynamics of the cylinder vibrating in a torsional flutter mode is considered, and compared to that of the stationary cylinder. The sectional distribution of the statistics of the pressure coefficients (mean, RMS, skewness and kurtosis) have been analysed, together with Probability Density Functions and the Power Spectra of the pressure fluctuations. Finally, the spanwise correlation of pressure fluctuations is investigated. Some of the modifications brought to the flow around the section by the addition of turbulence or by the motion of the cylinder have been inferred.*

1 INTRODUCTION

Simple sections such as the circle, the square and the rectangle constitute a fundamental repertoire in bluff bodies aerodynamics, whose relevance is due to two main reasons. First, they are elementary shapes, which allow investigating complex aerodynamic mechanisms, and comparing the results obtained using different tools. Second, these sections are found in many Civil and Mechanical Engineering structures (chimneys, towers, antennas, building, bridges, etc.) or structural components (rods, stays, etc.), therefore the results which are obtained in research find in many cases immediate application to design problems. These reasons prompted many researches in the last decades to investigate on aerodynamics of these sections.

In this paper, some issues associated with the aerodynamics of fixed and vibrating rectangular cylinders are discussed. Generally speaking, for a rectangular cylinder the statistics of pressures and aerodynamic forces, and the spanwise correlation of their fluctuations depend on the following parameters:

$$C_p = C_p \left(\frac{B}{D}, I_u, \frac{L_u}{D}, Re, \beta, \bar{h}, \tilde{h}.\bar{\alpha}, \tilde{\alpha}, U_{red} \right) \tag{1}$$

in which B/D is the breadth-to-depth ratio, representing the geometry of the section; I_u and L_u are the longitudinal intensity and integral scale of turbulence, respectively; Re is the Reynolds number; β is the blockage ratio; $\bar{h}, \tilde{h}, \bar{\alpha}, \tilde{\alpha}$ are mean and RMS values of the heaving and pitching motions, respectively; U_{red} is the reduced velocity, representing the vibration regime.

In Ref. [1] the aerodynamics of rectangular sections characterised by various breadth-to-depth ratios B/D between 0.6 and 8 were numerically investigated. The wide range of B/D ratios allowed pointing out the different types of behaviour occurring in the absence or presence of a reattachment of the shear layer. The relevant aerodynamic parameters (Strouhal number, Drag and Lift coefficients, distributions of mean and fluctuating pressures) were compared. In particular, discontinuities in the Strouhal number at the critical breadth-to-depth ratios $B/D = 2.8$ and $B/D = 6.0$ were pointed out. The Drag coefficients and the mean pressure distributions were in good agreement with the numerical results already available.

Among the first works on the effects of turbulence on the aerodynamics of rectangular cylinders are those of Refs. [2, 3, 4]. In Ref. [2] the effects of intensity and scale of turbulence were investigated on the mean pressure distributions around rectangular sections with B/D equal to 0.2, 0.4, 0.6 and 1, and on the spanwise correlation of the pressure fluctuations. The Reynolds number in the wind tunnel was $1.4\text{x}10^4$ to 10^5 based on the section depth, the intensity of turbulence was equal to 6% or 10%, and the integral scale ranged between $0.21D$ and $14D$. It was found that for very small values of B/D, small-scale turbulence tends to decrease the base pressure and to increase the strength of vortex shedding, while for larger values of B/D the effect reverses, with an increase in the base pressure and a decrease in the intensity of vortex shedding. On the other hand, large-scale turbulence has the effect of reducing the spanwise correlation of vortex shedding, thus increasing base pressure. The effect of the oncoming turbulence on the mean pressure distribution along the separation bubble formed on a flat plate with rectangular leading-edge were investigated in Ref. [3]. Wind tunnel tests were performed in grid-generated turbulence, with intensity of about 7% and 11%, and a longitudinal scale ranging between $0.5D$ and $24D$, at a Reynolds number of $1.4\text{x}10^4$ to $4.2\text{x}10^4$, based on the plate thickness. It was observed that the main effect of free-stream turbulence is to shorten the separation bubble, whose length decreases with increasing turbulence intensity. Furthermore, the mean pressure distribution along the separation bubble appears to be insensitive to changes in the turbulence scale up to $L_u = 2D$. Beyond that, the mean pressure distribution tends asymptotically to that associated with a smooth oncoming flow. Ref. [4] reports of

an investigation on the effects of turbulence on the mean flow past 2D and 3D bluff bodies, with square, rectangular and flat plate sections. The turbulent flow was characterized by a turbulence intensity of 6.6% and 12 %, and by a longitudinal scale of $0.3D$ to $24D$. Measurements were taken at Reynolds number in the range of $1.4\text{x}10^4$ to $2.8\text{x}10^4$. The tests showed that small-scale turbulence causes the separated shear layer to reattach to the side face earlier, while large-scale turbulence interacts with the shedding of vortices, thus changing the mean flow considerably. Another fundamental work was that of Ref. [5], in which the pressure fields around a rectangular cylinder with and aspect ratio $B/D = 6.67$ were studied, and some contradictions in the results available in the literature were pointed out. In particular, it was shown how it is impossible to distinguish the effects of large-scale turbulence from those due to small-scale turbulence, when the intensity is kept constant. This because to any increase in the large scale content implies a decrease in the small scale content.

Among the papers reporting the effects of the Reynolds number, Ref. [6] presents the results obtained on rectangular cylinders with breadth-to-width ratios of 2, 3 and 4, located in smooth and turbulent flow in a pressurized wind tunnel, at different angles of incidence. The Reynolds number was varied from $1.5\text{x}10^5$ to $4\text{x}10^6$, with a Mach number never exceeding 0.3. The results obtained are useful to define the influence of Reynolds number, after-body length, angle of attack and turbulence of the approaching flow, on the aerodynamics of rectangular cylinders. In particular, Reynolds number effects on the mean Drag and Lift were observed, this effects varying with the intensity of turbulence and Mach number regime.

On the other hand, the frequency and amplitude dependency of the aerodynamic action on oscillating cylinders has been widely investigated over the decades, both from the theoretical point of view and for practical applications. It is known that this dependency is the result of the existence of motion related forces, whose characteristics change with the vibration regime. However, motion dependent forces are one component of the overall excitation. This turns out to be the combination of different mechanisms that in some cases simply superimpose, while in some others strongly interact with each other. Separation of the different components contributing to the overall aerodynamic force is of interest for a better understanding of the physics underlying the problem, and for the purpose of modelling the aerodynamic action.

The relationship of the aerodynamic forces to the torsional vibration of rectangular cylinder with $B/D = 5$ was investigated numerically in Ref. [7], through solution of the Navier-Stokes equations. The existence of a pronounced shedding-induced interaction for values of the reduced wind speed between 1 and 2 (based on the section breadth) was recognised, together with a torsional flutter instability at a reduced wind speed of 6. The mechanisms of fluid-structure interaction were also investigated through the analysis of the work done by the aerodynamic pressures. On the other hand, the existence was pointed out in Ref. [8] of two types of vortex shedding flow instabilities on stationary rectangular cylinders, whose occurrence is related to the breadth-to-width ratio of the section. A comprehensive classification of possible aeroelastic instabilities of cylinders is given in Ref. [9]. The distribution of the unsteady pressures for different breadth-to-width ratios is also analysed by means of wind tunnel tests, together with its effects on flutter derivatives. The derivation of flutter derivatives from the unsteady pressure distributions allows interpretation of the different flutter mechanisms and of the fluid dynamics reason of their occurrence. In Ref. [10] the results of the application of Proper Orthogonal Decomposition (POD) to the pressure fluctuations measured in the wind tunnel on an oscillating bridge box section model are discussed. It was found that POD allows decoupling the force components associated with the different excitation mechanisms coexisting on the vibrating cylinder. More generally, Ref. [11] discusses the possibility of applying POD to pressure fluctuations, as a tool to investigate the mechanisms of wind loading of structures.

(a)

(b)

Figure 1: a) Model in the test section; b) Suspension system in the aeroelastic tests.

Besides the characteristics of sectional forces, in the analysis of the aeroelastic response of cylinders it is relevant how the aerodynamic action correlates spanwise. In Ref. [12] the results of wind tunnel measurements on a fixed rectangular cylinder with $B/D = 5$ are discussed. The cylinder upper face was provided with 342 pressure taps, arranged in 18 arrays of 19. This allowed the analysis of the spanwise coherence of pressure fluctuations at different locations on the side face of the section. Finally, in Ref. [13] the results of similar measurements are shown for a vibrating cylinder with the same breadth-to-width ratio, through the analysis of the spanwise correlation functions of the aerodynamic forces and of the stagnation and base pressures. It was pointed out that for increasing separation the correlation functions tend to a non-zero value for all vibrations regimes. This indicates the existence of a fully correlated portion of the aerodynamic force, which in some cases is as large as 89% of the total fluctuating force.

In this paper the results of wind tunnel tests are shown, aimed at the analysis of the pressure distributions and spanwise pressure correlation on a 5:1 rectangular cylinder in smooth and turbulent flow. In addition, limited to the smooth flow regime, a comparison between the pressure distributions on the fixed cylinder and on the cylinder vibrating in a torsional flutter are also shown.

2 WIND TUNNEL TESTS

Wind tunnel tests were carried in the CRIACIV (Inter-University Research Centre for Building Aerodynamics and Wind Engineering) boundary layer wind tunnel in Prato, Italy. The open circuit wind tunnel has a total length of about 22 m, and a test section of 2.40 m x 1.65 m with an upstream fetch of about 8 m. The target wind speed, in the range of 0 to 35 m/s, is obtained by means of both the adjustment of the fan rotation speed and of the pitch of the 10 blades. The 2.32 m long rectangular model, with a cross section of 30 cm x 6 cm was placed in the 2.40 m wide test section, with the suspension system located outside the tunnel (Fig. 1).

The model was made of carbon fibre composite to minimise the weight, and is provided with 342 pressure taps arranged in eight sectional arrays (seven of 30 and one of 52 pressure
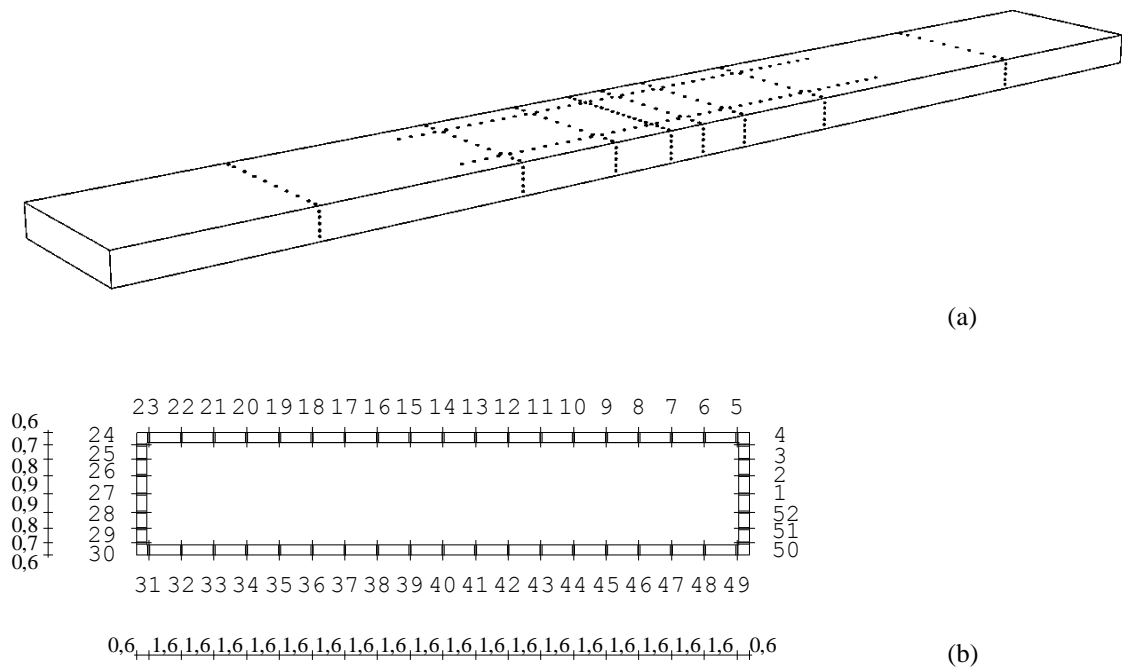
(a)

(b)

Figure 2: a) 3D sketch of the model with pressure tap location; b) instrumented cross section with 52 taps

taps) and two longitudinal arrays of 40 taps, as shown in Fig. 2. The array of 52 taps was used for characterisation of the sectional aerodynamic forces, the arrays of 30 taps were used to investigate the spanwise correlation of the forces, and the two longitudinal arrays were used to characterise the short distance spanwise correlation of pressure fluctuations. Six high frequency pressure scanners were located inside the model and connected to the acquisition system located outside the tunnel.

Two different suspension systems were used, the first being a stiff rig for static tests. In a second stage aeroelastic tests were carried out providing the model with the heave and pitch degrees of freedom. The parameters of the dynamic setup are a mass and a mass moment of inertia of the model of 15.13 Kg and 0.222 Kg x m^2, respectively. These include model, scanners with tubing and wires, supporting arms and the modal contribution of the springs. This led to vibration frequencies of 4.3 Hz and 7.1 Hz in the heave and pitch degrees of freedom, respectively, with a ratio of 1.65.

In addition to the pressure measurements, in the static tests six load cells were used to measure the total aerodynamic forces, and in the dynamic tests three laser displacement transducers were used to measure the model instantaneous displacements.

Measurements were taken in smooth flow at a reference wind velocity of 15.9 m/s, corresponding to a Reynolds number of 63600 (based on the model depth), and in grid-generated turbulent flow at a reference mean wind velocity of 11.3 m/s, corresponding to a Reynolds number of 43100. The intensity and integral scale of the longitudinal component of turbulence were I_u=0.17 and L_u=21 cm (L_u/B=0.7), respectively. Pressures were sampled at 250 Hz, and the sampling time was 270 s in the static tests and 240 s in the dynamic tests. The displacements were sampled at 1000 Hz for 240 s.

For the particular breadth-to-width ratio of 5 considered, the three vibration regimes of buffeting, shedding induced vibration and flutter manifest themselves, depending on the reduced wind speed. In smooth flow a dominant shedding induced heaving vibration was found
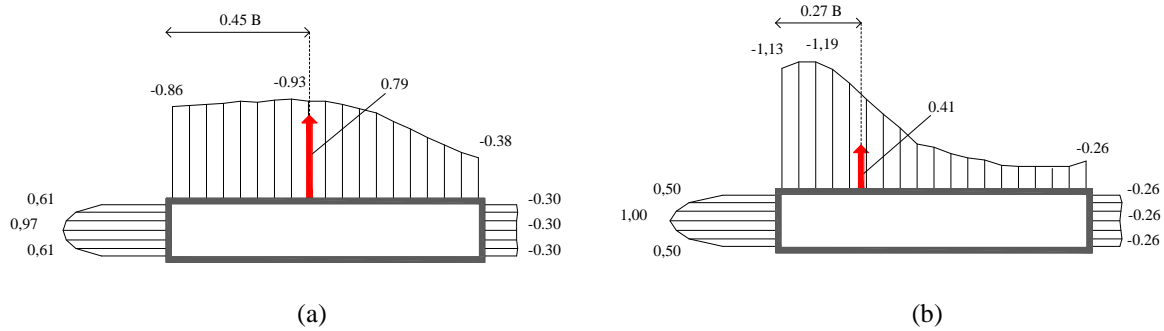
5

Figure 3: Mean pressure coefficient sectional distribution in smooth (a) and in turbulent flow (b).
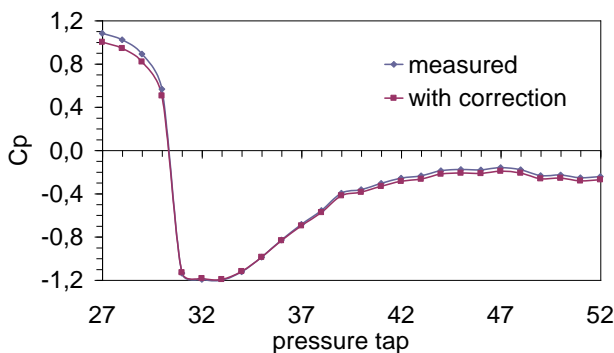

Figure 4: Comparison between the measured and corrected mean pressure coefficients in turbulent flow.

for a value of the reduced wind speed of about 1.55 (based on the model breadth and on the heaving frequency), a dominant shedding induced pitching vibration for values of the reduced wind speed of about 1.25 (based on the pitching frequency), and a torsional flutter with a on-set reduced speed in the range of 4.7 (based on the pitching frequency). At other values of the wind speed the model vibration was associated with the effects of signature turbulence. To-gether with the results of the static tests, in this paper only the results concerning the flutter vibration regime will be presented.

3 PRESSURE DISTRIBUTIONS AND AERODYNAMIC FORCES ON THE STATIONARY CYLINDER

The sectional distributions of the mean pressure coefficients on the stationary cylinder in smooth and turbulent flow are shown in Fig. 3. The pressure coefficients shown for the smooth flow condition are those calculated with respect to the static and dynamic pressures measured with the Pitot tube. For the turbulent flow condition, on the other hand, the pressure coefficients have been corrected to compensate for the non perfectly uniform distribution of the mean wind velocity in the tunnel. The correction consists in setting the mean stagnation pressure coefficient equal to one, and keeping constant the sum of the static and dynamic wind pressures. To give an idea of the correction applied, in Fig. 4 the measured and corrected mean pressure coefficients are shown.

The main effects of turbulence consist in the increase of magnitude of the negative pres-sure peak on the side faces, and in its displacement towards the leading edge. In particular, the
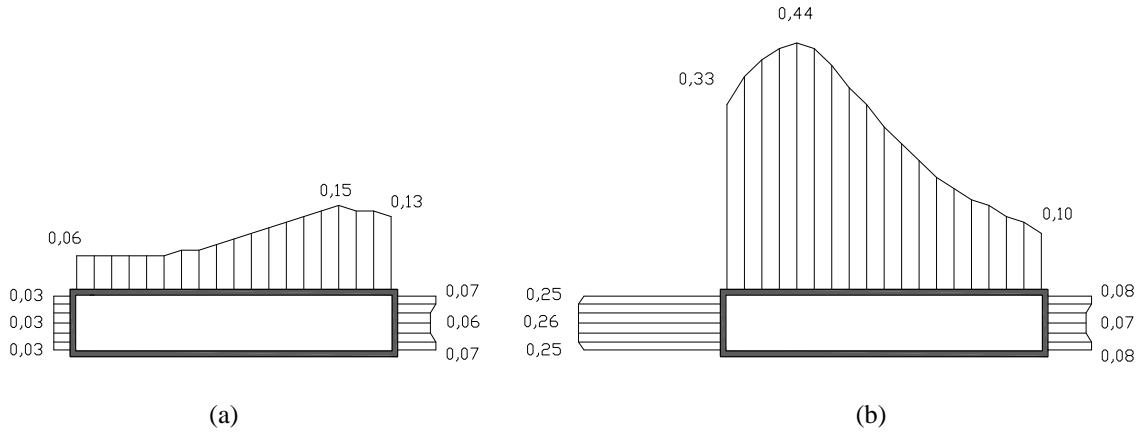
Figure 5: RMS pressure coefficient sectional distribution in smooth (a) and in turbulent flow (b).

minimum pressure coefficient in smooth flow is -0.93, and it is located 0.39B downstream the leading edge, while in turbulent flow the minimum pressure coefficient is -1.19, and it is located 0.13B downstream the leading edge. Downstream the point on minimum mean pressure, the negative pressure drops much faster in turbulent flow than in smooth flow, to values that can be as low as -0.19, while in smooth flow the negative pressure coefficient is never lower than -0.38. In Fig. 3 the position and magnitude (in terms of force coefficient) of the total action on each lateral face is also shown. In smooth flow the resultant on each lateral face is located 0.45B downstream the leading edge, and has an associated force coefficient of -0.79. In turbulent flow it moves to a point located 0.27B downstream the leading edge, and the associated force coefficient is -0.41.

The sectional distributions of the RMS pressure coefficients on the stationary cylinder in smooth and turbulent flow are shown in Fig. 5. Besides the increase in pressure fluctuations on the windward face, which is associated with the direct effect of the oncoming turbulence, a strong increase of pressure fluctuations on the lateral faces is observed, especially at points located towards the leading edge of the section.

Understanding of the modifications brought to pressure fluctuations by the addition of turbulence can be gained looking at the pressure spectra shown in Fig. 6. As expected at the stagnation point the spectrum of the pressure fluctuations in turbulent flow is very much close to the spectrum of the oncoming turbulence, as opposed to a quite flat spectrum measured in smooth flow. At the location of tap 8, i.e. 0.82B downstream the leading edge, and at the base point the pressure fluctuations in smooth flow are mainly concentrated at a reduced frequency $fB/U = 0.58$, therefore they are the result of vortex shedding occurring with a depth-based Strouhal number of 0.116. In turbulent flow the magnitude of the pressure fluctuations doesn't change (in smooth flow $\tilde{C}_p = 0.15$ and $\tilde{C}_p = 0.06$ at tap 8 and at the base point, respectively, and $\tilde{C}_p = 0.15$ and $\tilde{C}_p = 0.07$ in turbulent flow), but the pressure fluctuations seem to be no more associated to a pronounced vortex shedding, but rather to broadband wake fluctuations. Finally, at the location of tap 19, i.e. 0.23B downstream the leading edge, the pressure fluctuations dramatically increase in turbulent flow, with a RMS pressure coefficient going from 0.06 in smooth flow to 0.44 in turbulent flow. Looking at the spectra of the pressure fluctuations shown in Fig. 6, one can conclude that such an increase is primarily associated with broadband pressure fluctuations of the separation bubble.

Finally, the distribution of the RMS pressure coefficients on the side faces proves steeper
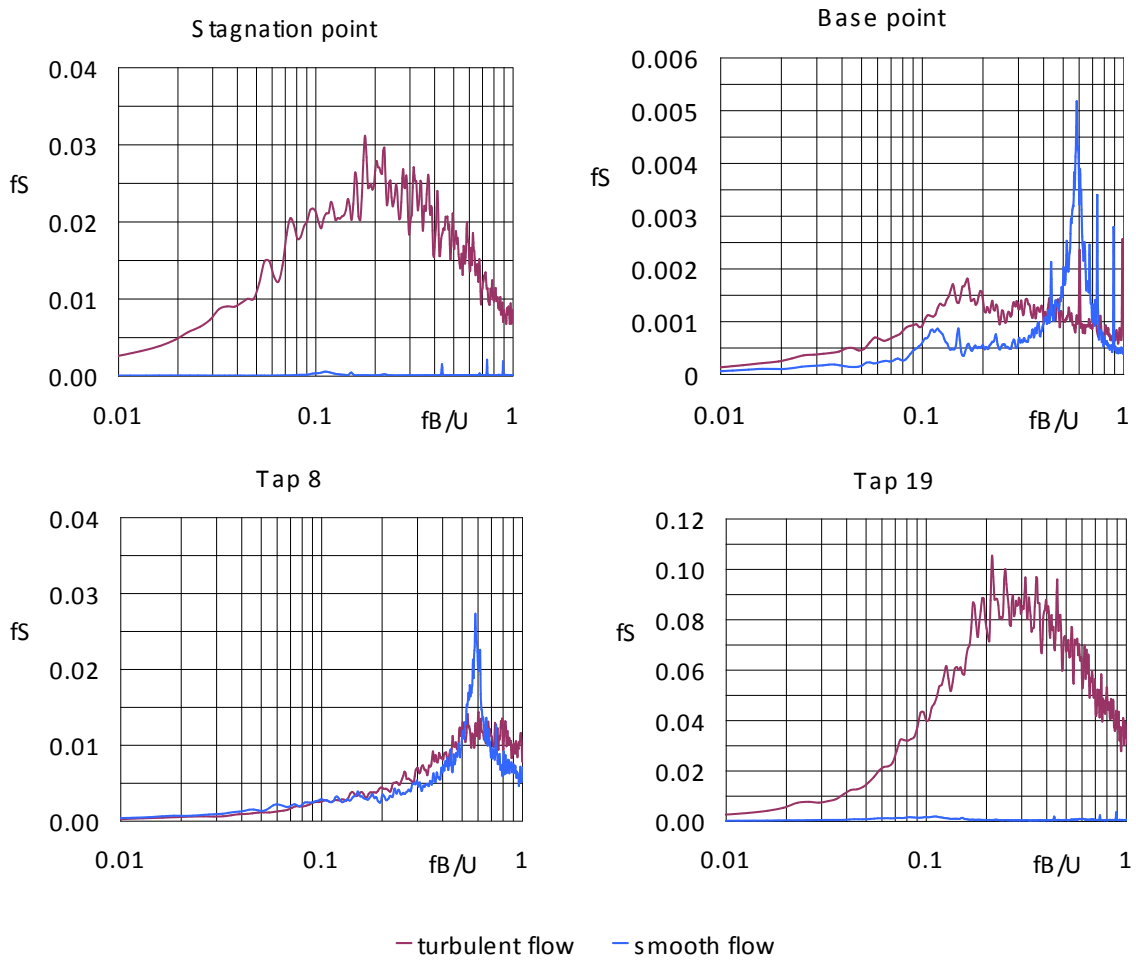
Figure 6: Power Spectral Density functions of pressures at four locations in smooth and in turbulent flow.

in turbulent flow than in smooth flow, and this can be caused by the faster pressure recovery occurring in turbulent flow. The reason for this type of behavior may be sought in the position of the reattachment point of the separated shear flow. The reattachment point proves to be in turbulent flow closer to the leading edge than it is in smooth flow. The position of the reattachment point can be evaluated based on the distribution of the mean and RMS pressure coefficients. In particular, it can be reasonably assumed that this position is at the midpoint between the minimum value of the mean pressure and that of the maximum value of the RMS pressure. Under this assumption, the reattachment point would be located $7.2/8B$ downstream the leading edge in smooth flow, and $4.4/8B$ in turbulent flow. The value calculated for the smooth flow condition appears to be in good agreement with the value given in Ref. [12] of $7/8B$, while the discrepancy appearing in turbulent flow ($3/8B$ is the value given in Ref. [12]) is mainly attributed to the difference in the characteristics of the oncoming turbulent flow, and to the possible differences in the method used to find the reattachment point in Ref. [12].

In order to evaluate the distance between the Gaussian hypothesis and the real behavior of the pressures fluctuations, the pressure skewness and kurtosis were evaluated for the smooth and turbulent flow conditions. The coefficient of skewness:

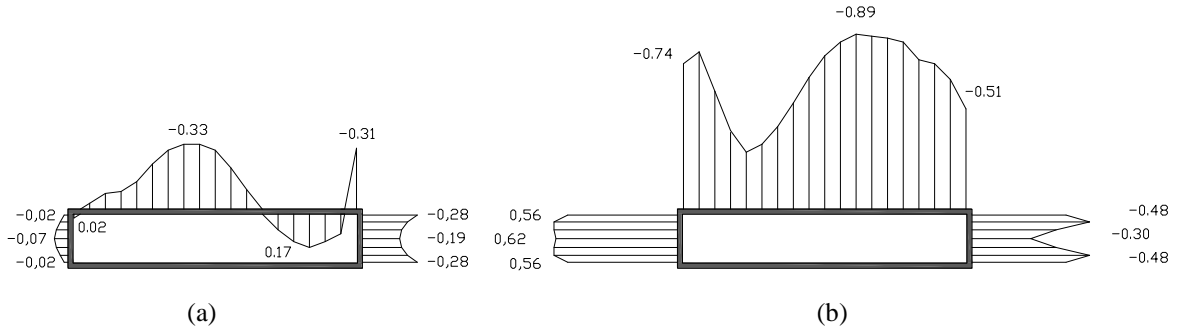$$g_1 = \frac{m_3}{m_2^{3/2}} \tag{2}$$

8

(a)   (b)

Figure 7: Sectional distribution of the pressure skewness coefficient in smooth (a) and in turbulent flow (b).

with m_j indicating the j-th moment of the distribution:

$$m_j = \frac{1}{N} \sum_{i=1}^{N} \left(C_p(t_i) - \bar{C}_p \right)^j \tag{3}$$

gives a measure of the symmetry of a distribution. It is positive when a unimodal distribution has a dominant right tail, while it is negative when the distribution has a dominant left tail. A nil value characterises a symmetric distribution. The coefficient of kurtosis:

$$g_2 = \frac{m_4}{m_2^2} \tag{4}$$

represents the degree of flattening of a distribution near its peaks. In a unimodal distribution, a value of the kurtosis coefficient larger than 3 implies a sharper peak in the neighborhood of the mode than that of a Gaussian distribution having the same RMS, whereas a value lower than 3 implies a flatter peak. In Eq. (3) $C_p(t_i)$ is the value of the pressure coefficient at time t_i, $\bar{C}_p$ is the mean value of the pressure coefficient, and N is the number of sampling instants.

The sectional distribution of the skewness coefficients is shown in Fig.7. Except for a few points in the smooth flow condition, it appears that the pressure fluctuations are away from being symmetric, with the asymmetry increasing with the addition of turbulence. To illustrate this feature, in Fig. 8 the Probability Density Functions (PDFs) of the pressure fluctuations at the stagnation and base points, and at the location of taps 8 and 19, are shown, as measured in smooth and turbulent flow. As a reference, in the plots also the corresponding Gaussian distribution is shown.

At the stagnation point in smooth flow pressure fluctuations are the result of minor flow fluctuations in the wind tunnel and, primarily, of the unsteady flow associated with wake fluctuations. This makes the PDF of the aerodynamic pressure quite narrow and symmetric. However, the addition of turbulence has the effect of making the PDF of the pressure much broader and skewed to the left (longer right tail). Under the assumption of a Gaussian oncoming turbulence, this is the effect of the quadratic pressure term associated with turbulent fluctuations.

On the other hand the addition of turbulence brings only minor modifications to the PDF of the pressures on the leeward face of the section. Besides the variation in the mean pressure, at the base point, turbulence makes the PDF skewed to the right, and this phenomenon is even more pronounced at points on the leeward face closer to the edges. This does not derive from an increase in the pressure fluctuations (as the RMS values do not change), therefore it has to be the result of the modification produced by turbulence of the characteristics of the wake.
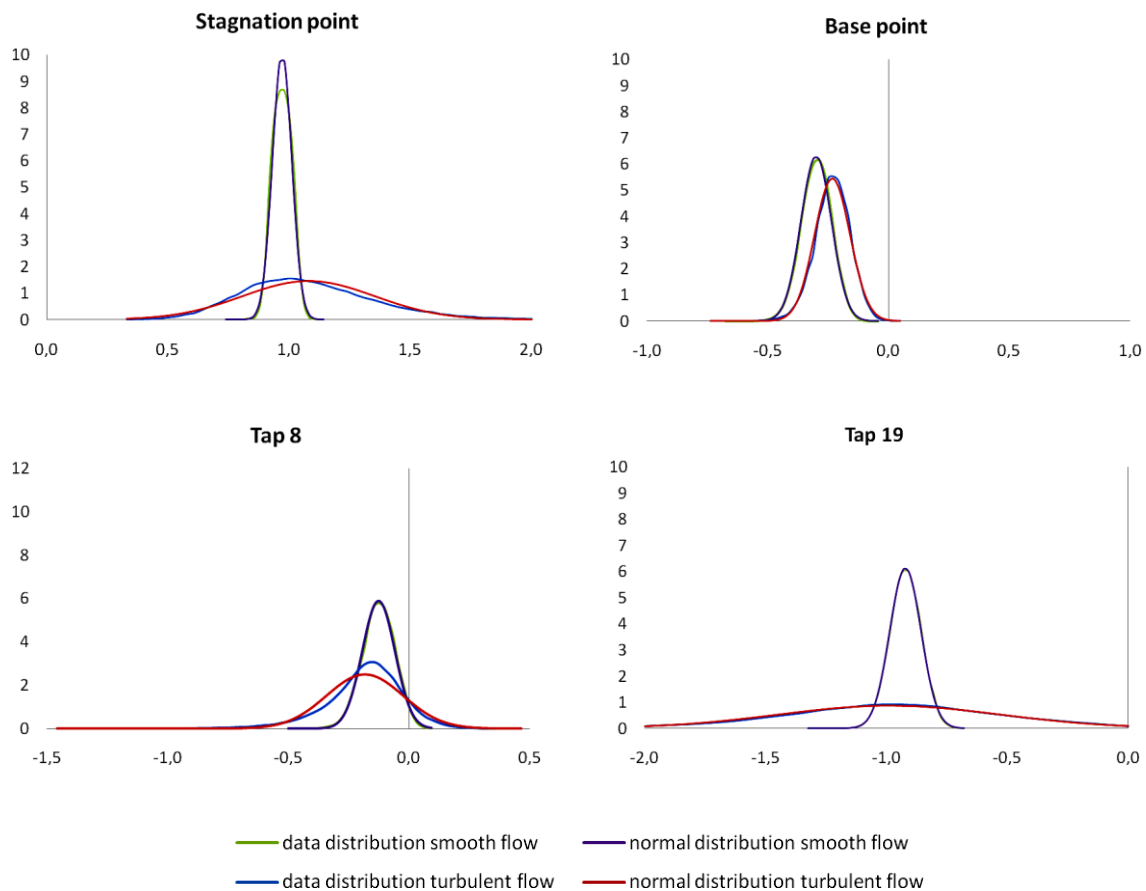
9

Figure 8: Probability Density Functions of the stagnation and base pressures and of the pressures at taps 8 and 19, in smooth and turbulent flow.

Finally, the addition of turbulence completely modifies the PDFs of the pressure fluctuations on the side faces of the section. From Fig. 7 it can be seen that in smooth flow the skewness of pressure fluctuations is negative up to a point located at $2/3B$ downstream the leading edge, and then becomes positive, to finally become negative again at the trailing edge. On the other hand, in turbulent flow the skewness is always negative, and takes much larger values than in smooth flow. A negative skewness in turbulent flow is the effect of the fluctuations of suction on the side faces. These are associated with the fluctuations of the oncoming flow, which produce larger suction peaks, therefore skews the pressure PDF to the right. It is also observed that the maximum skewness is reached $5.6/8B$ and $1.9/8B$ downstream the leading edge in smooth flow and turbulent flow, respectively. In both cases the maximum skewness is reached upstream the reattachment point, therefore towards the end of the separation bubble.

In Fig. 8 the PDF of pressures at taps 8 and 19 are shown, corresponding to the points of maximum skewness in smooth and turbulent flow, respectively. At tap 8, the skewness takes the positive value of 0.17 for the reason postulated above; when turbulence is added, the reattachment point moves upstream and the measurement point gets out of the separation bubble. Pressure fluctuations in this case are no more associated with pulsing reattachment, but rather with the rolling of vortices. This has the effect of skewing the PDF to the right, with a negative skewness coefficient of -0.76. At tap 19, there is a low negative skewness of -0.14 in smooth flow; the addition of turbulence skews to the right the PDF of the pressures at all points on the side faces; however at the location of tap 19 this effect is minimum.
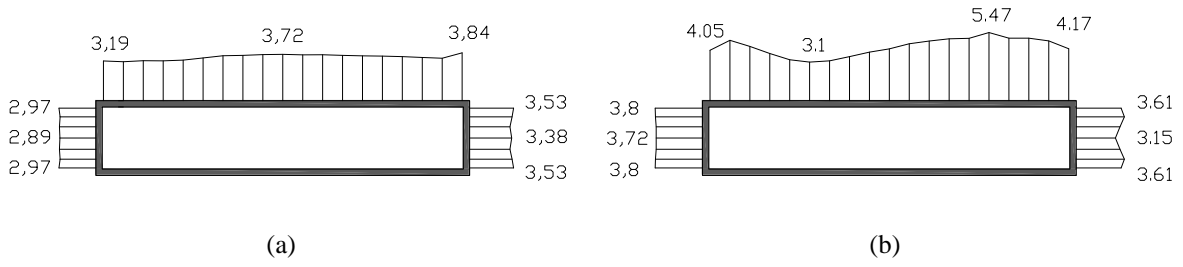
Figure 9: Sectional distribution of the pressure kurtosis coefficient in smooth and in turbulent flow.

Finally, the sectional distribution of the kurtosis coefficient is shown in Fig. 9. In smooth flow the sharpness of the PDF of the pressures on the windward face of the section is very close to that of a Gaussian distribution, with a kurtosis coefficient very close to 3. On the leeward and on the side faces the peak tends to be slightly flatter, but the kurtosis coefficient never exceeds the value of 3.84, 28% larger than for a Gaussian distribution. In turbulent flow, however, the peak of the pressure PDF becomes flatter almost everywhere on the section, with values of the kurtosis coefficient as large as 5.47, 82% larger than for a Gaussian distribution.

The largest kurtosis is associated with the maximum skewness, and it occurs in turbulent flow on the leeward half of the side faces. These are the points in which the pressure fluctuations are most away from a Gaussian behaviour. As earlier pointed out, in turbulent flow this portion of the section is subject to the rolling of vortices shed at the leading edge, which my cause the pressure fluctuations to be away from those that would derive from the turbulent fluctuations of the oncoming flow.

4 SPANWISE PRESSURE CORRELATION

In Ref. [13] the spanwise correlation of the aerodynamic forces and of the stagnation and base pressures on a stationary and vibrating 5:1 rectangular cylinder in smooth flow were analysed.

The correlation coefficient:

$$R_{C_p}(\delta/D) = \text{cov}\left[C_p(\delta/D)\right]\big/\tilde{C}_p^2 \tag{5}$$

δ being the separation between the two points of measurement, was calculated from the measured data.

The data were interpolated through the equation:

$$R_{C_p}(\delta/D) = \exp\left[-c\cdot\left(\delta/D - k\right)\right] + d \tag{6}$$

which accounts for the correlated portion d of the aerodynamic pressures and forces existing on the vibrating cylinder. For the stationary cylinder $d = k = 0$, and eq. (6) reduces to a simple negative exponential. For the stagnation and base pressures values of the decay coefficient of 0.952 and 0.526 were found, respectively.

In this case, similar measurements were taken, in smooth and turbulent flow, at two points on the side face of the section, located 0.18B (array α) and 0.82B (array β) downstream the leading edge. The results of the measurements are shown in Fig. 10, together with their exponential interpolations. There resulted exponential decay coefficients of 0.228 and 0.215 for the array α in smooth and turbulent flow, respectively, and of 0.532 and 0.496 for the array β in smooth and turbulent flow, respectively.

When one compares the results obtained here with those of Ref. [13], it can be concluded that the maximum correlation occurs at the location of the array α, i.e. inside the separation
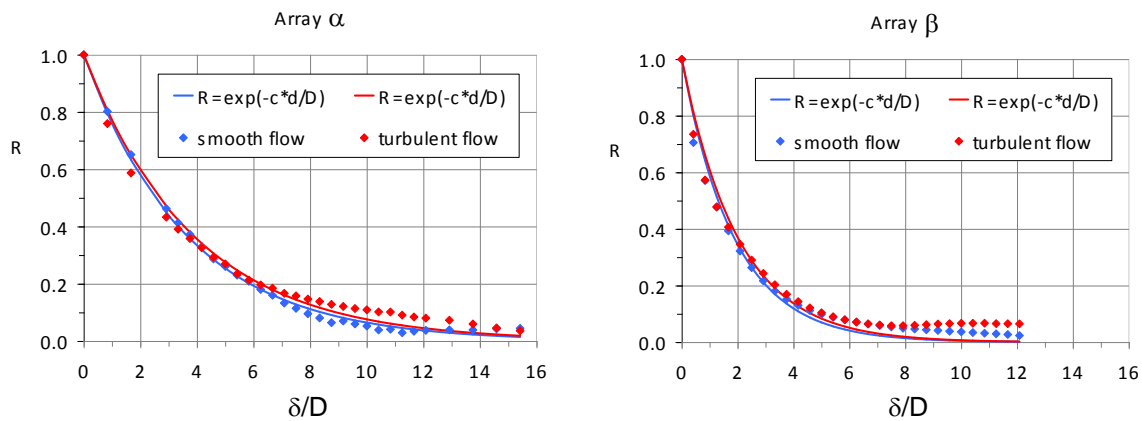
Figure 10: Cross correlation coefficient of pressures at two longitudinal arrays in smooth and in turbulent flow.

bubble. A similar result is also shown in Ref. [12]. The minimum correlation, on the other hand, was measured at the stagnation point, where pressure fluctuations in smooth flow are associated with signature turbulence, therefore are of small magnitude and small size. At the location of the array β and at the base point, the spanwise pressure correlations are comparable. This because at both locations pressure fluctuations are associated with the wake dynamics, therefore having the same nature.

When the correlation at the location of the arrays α and β measured in smooth and turbulent are compared, it is found that these are quite similar to each other. This result tells that on the side faces of the section, where the pressure fluctuations are governed by the separated flow, even though the flow is modified by the addition of the oncoming turbulence, the spanwise correlation is not much affected by these modifications.

5 PRESSURE DISTRIBUTIONS AND AERODYNAMIC FORCES ON THE VIBRATING CYLINDER

When the cylinder is not stationary (either because externally driven into motion, or because elastically supported and excited by the wind) the surface pressure distribution is known to be different from what it is on the stationary cylinder. In addition, the pressure distribution depends on the amplitude of the oscillation and on the vibration regime, i.e. on the reduced wind velocity. As mentioned in section 2, measurements were taken on the model free to vibrate in the heaving and pitching degrees of freedom, for values of the reduced wind speed in the range of 0.64 to 7.8, with respect to the heaving natural frequency (0.4 to 4.7 with respect to the pitching natural frequency). In particular, at a reduced velocity (with respect to the pitching frequency) of 4.1, the model goes into a torsional flutter instability, vibrating at a frequency of 6.9 Hz, 3% lower than the vibration frequency in still air. In the following a comparison will be made, for a smooth oncoming flow, between the characteristics of the pressures on the stationary cylinder and those on the cylinder vibrating in a torsional flutter regime, at a reduced wind velocity of 4.7, at an RMS amplitude of 1.87° (the RMS amplitude in the heaving mode being 0.47 mm).

In Fig. 11 a comparison is made between the sectional distribution of the statistics of the pressure coefficients on the stationary and vibrating cylinder. It can be noticed that the vibration does not change much the mean pressure distribution. This result is acceptable because of the symmetry of the section, oscillating with respect to a symmetric configuration, but it also indicates that in spite of the vibration the mean flow around the section isn't heavily modified.
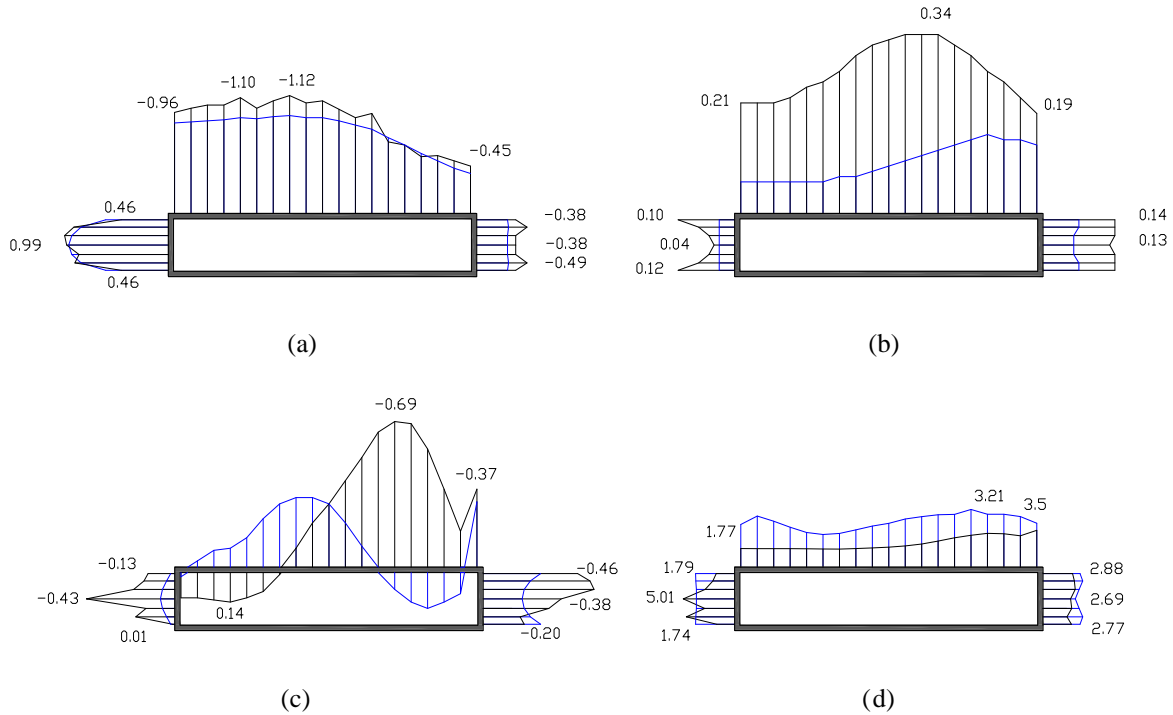
Figure 11: Sectional distribution of the pressure statistics on the stationary cylinder (blue) and on the cylinder vibrating in a torsional flutter (black); mean (a), RMS (b), skewness (c) and kurtosis (d).

On the other hand, as expected the distribution of the RMS pressures at flutter is everywhere larger than on the stationary cylinder. In particular, it is found that to a uniform RMS pressure distribution on the windward face on the stationary cylinder, a strongly variable distribution corresponds at flutter. The latter has about the same value of the RMS stagnation pressure coefficient than on the stationary cylinder (0.04 versus 0.03), however at flutter the pressure fluctuations increase as the edge of the cylinder is approached, with RMS pressure coefficients that get as high as 0.12. This behaviour can be justified as the effect of the acceleration of the flow at the edge of section, occurring with varying pitching angle. The fluctuating pressures on the leeward face remain almost constant, but their RMSs are almost doubled with the torsional vibration. Finally, the pressure fluctuations on the side faces are more than doubled. Their space distribution approximately does not change in shape, but the point of maximum RMS pressures moves upwind to a position located $0.61B$ downstream the leading edge (as opposed to $0.82B$ measured on the stationary cylinder). If the same rule of Section 3 is used to find the point of reattachment of the flow, this is found to be located at $6.4/8B$ from the leading edge, as opposed to $7.2/8B$ which applies to the stationary cylinder. This suggests that the average size of the separation bubble on the vibrating cylinder is smaller than that of the stationary cylinder. The nature of the pressure fluctuations on the vibrating cylinder is quite different with respect to that of the pressure fluctuations on the stationary cylinder, as the former are governed by the motion. In Fig. 12 the PSDs of the stagnation and base pressure fluctuations are shown for the vibrating cylinder, together with those of the pressure fluctuations at taps 8 and 19, and compared with those of the stationary cylinder. It is noticed that all the spectra are dominated by a sharp peak at a reduced frequency of 0.21, corresponding to the vibration frequency of 6.9 Hz, and by smaller peaks at the first two harmonics of the vibration frequency. This makes it clear that the fluid dynamics, therefore the pressure fluctuations are governed by the motion.
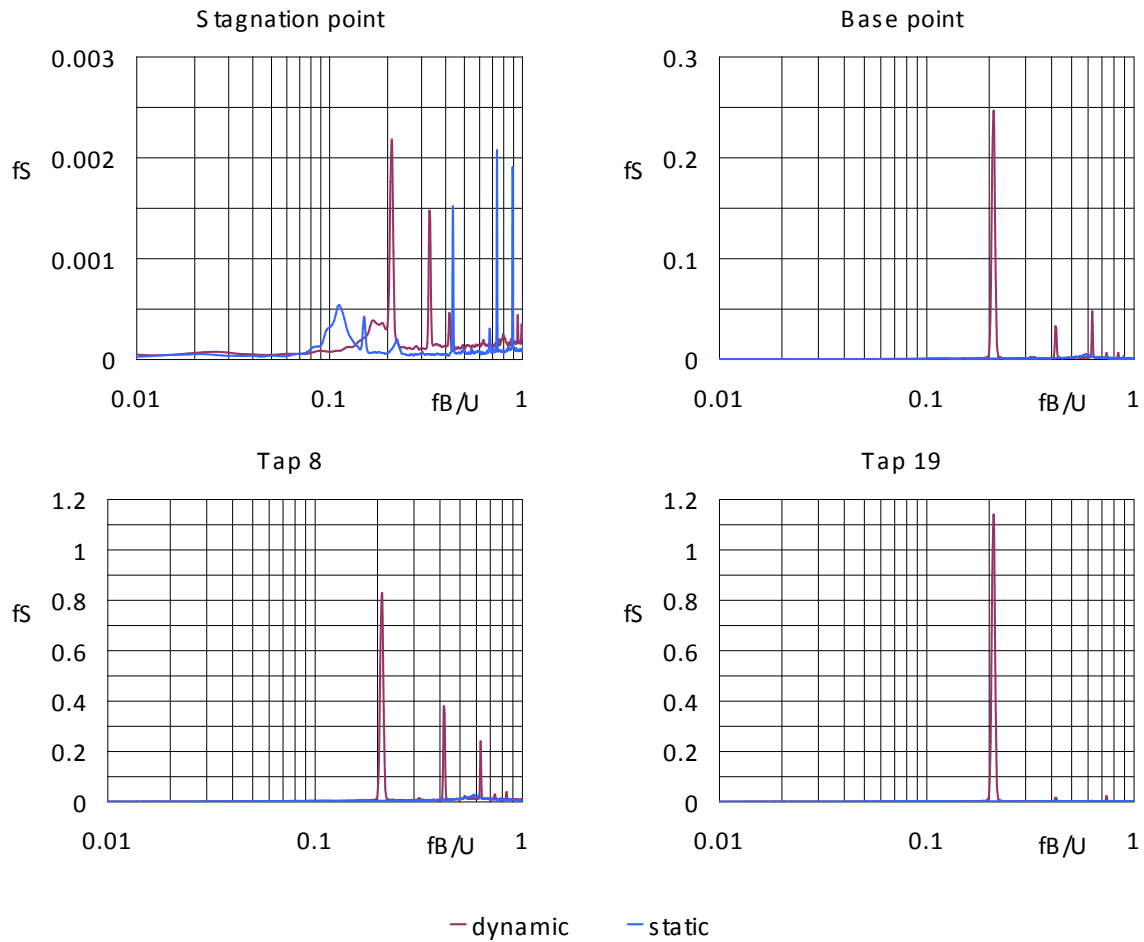
13

Figure 12: Power Spectral Density functions of pressures at four locations on the stationary and vibrating cylinder in smooth flow

The skewness of the pressure fluctuations (Fig. 11) is also globally increased at flutter, and its space distribution is modified. This is the effect of a dramatic change occurring to the PDFs of the pressure fluctuations. These are shown in Fig. 13 for the stagnation and base points, and for taps 8 and 19 in the form of histograms. At the stagnation point and at tap 8 the PDFs of the pressure fluctuations are skewed to right, giving rise to a negative value of the skewness coefficient. At both the base point and at tap 19, however, the pressures appear to have a bimodal distribution, which is quite consistent with the narrowband pressure fluctuations described by the peaky spectra of Fig. 12.

Finally, the kurtosis coefficient (Fig. 11) is everywhere lower than for the stationary cylinder, except for the stagnation point. This in most cases is the result of the bimodal PDF of the pressure fluctuations on the vibrating cylinder.

6 CONCLUSIONS

The distributions of the pressure statistics around a 5:1 stationary rectangular cylinder have been presented, as measured in smooth and turbulent flow. As expected these are quite different from each other, due to modification brought by turbulence to the flow around the body.

In particular it is found that in turbulent flow the pressure distribution on the side faces has larger suctions towards the leading edge than in smooth flow, and a faster pressure recovery
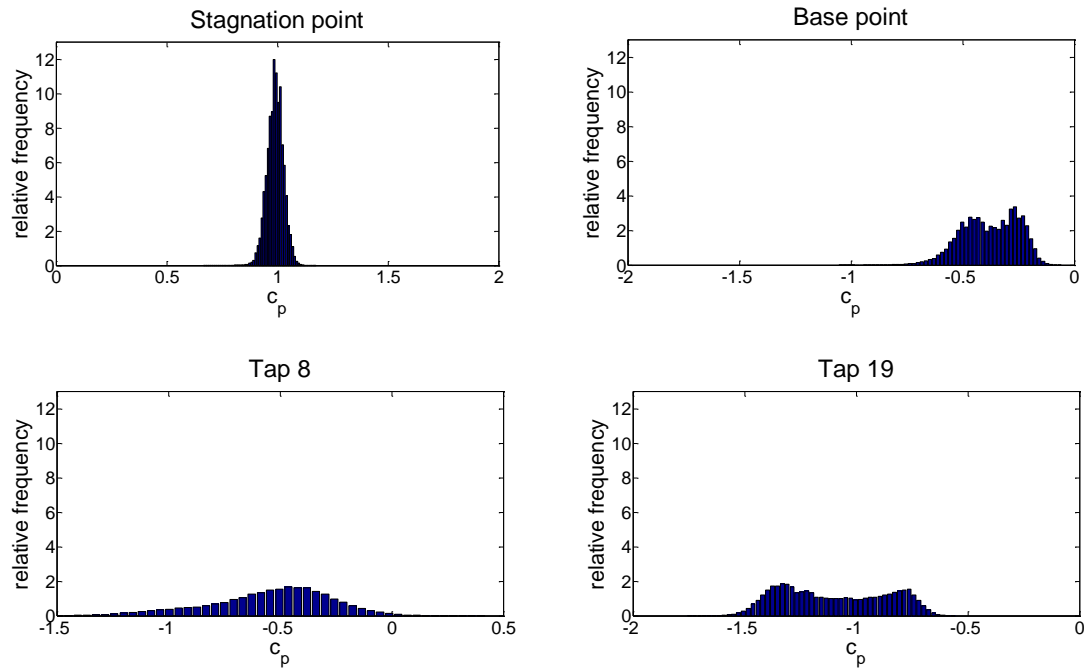
14

Figure 13: Histograms of the probability of the stagnation and base pressures and of the pressures at taps 8 and 19 on the vibrating cylinder.

towards the trailing edge. The pressure fluctuations increase at all points on the side faces, especially towards the leading edge. This indicates the smaller length of the separation bubble in turbulent flow, and the displacement of the reattachment point towards the leading edge. The pressure spectra at the stagnation and base point, and at locations on the side faces show the different nature of the surface pressure fluctuations in turbulent flow with respect to those in smooth flow. In particular, the pressure fluctuations which in smooth flow are associated with the wake dynamics tend to disappear in turbulent flow, replaced by broad band fluctuations associated with the turbulence of the oncoming flow.

The distributions of the pressure skewness and kurtosis coefficients, together with the PDFs of the pressures show that turbulence tends to make the surface pressures less Gaussian then they are in smooth flow, at almost all locations on the cylinder.

Only for the case of a smooth oncoming flow, a comparison is made between the statistics of the sectional pressure distribution on the stationary cylinder and those measured on the cylinder vibrating in a torsional flutter mode. Comparison has shown that the mean pressures at flutter are almost the same as those on the stationary cylinder. The pressure fluctuations, on the other hand, are higher than those on the stationary cylinder, and the nature of the fluctuations is quite different. In particular it is found that most of the fluctuation are of a self excited nature, making the external excitation almost negligible. In addition, the PDFs of the pressures on the vibrating cylinder are bimodal on the leeward portion of the side faces and on the leeward face, which is consistent with the narrow spectrum of the pressure fluctuations at these locations.

Finally, the spanwise correlation of pressures at two locations on the side faces of the stationary cylinder was investigated. Through comparison with results previously obtained it was found that the largest correlation exists at points within the separation bubble.

REFERENCES

[1] K. Shimada, T. Ishihara. Application of a modified $k - \varepsilon$ model to the prediction of aerodynamic characteristics of rectangular cross-section cylinders. *Journal of Fluids and Structures,* **16**, 465-485, 2002.

[2] Y. Nakamura, Y. Ohya. The effects of turbulence on the mean flow past two-dimensional rectangular cylinders. *Journal of Fluid Mechanics*, **149**, 255-283, 1984.

[3] Y. Nakamura, S. Ozono. The effects of turbulence on a separating and reattaching flow. *Journal of Fluid Mechanics,* **178**, 477-490, 1987.

[4] Y. Nakamura, Y. Ohya, S. Ozono. The effects of turbulence on bluff-body mean flow. *Journal of Wind Engineering and Industrial Aerodynamics*, **28**, 251-259, 1988.

[5] F.L. Haan jr., A. Kareem, A.A. Szewczyk. The effects of turbulence on the pressure distribution around a rectangular prism. *Journal of Wind Engineering and Industrial Aerodynamics*. **77-78**, 381-392, 1998.

[6] G.L. Larose, A. D'Auteuil. Experiments on 2D rectangular prisms at high Reynolds numbers in a pressurised wind tunnel. *Journal of Wind Engineering and Industrial Aerodynamics*, **96**, 923-933, 2008.

[7] T. Tamura, Y. Itoh, A. Wada, K. Kuwahara. Numerical study of pressure fluctuations on a rectangular cylinder in aerodynamic oscillation. *Journal of Wind Engineering and Industrial Aerodynamics*, **54-55**, 239-250, 1995.

[8] Y. Nakamura, Y. Ohya, S. Ozono, R. Nakayama. Experimental and numerical analysis of vortex shedding from elongated rectangular cylinders at low Reynolds numbers 200-l03, *Journal of Wind Engineering and Industrial Aerodynamics*, **65**, 301-308, 1996.

[9] M. Matsumoto. Aerodynamic damping of prisms. *Journal of Wind Engineering and Industrial Aerodynamics*, **59**, 159-175, 1996.

[10] F. Ricciardelli, E.T. de Grenet, G. Solari. Analysis of the wind loading of a bridge deck box section using Proper Orthogonal Decomposition. *Journal of Fluid Mechanics Research*, **29**(3-4), 312-322, 2002.

[11] F. Ricciardelli. Proper Orthogonal Decomposition to understand and simplify wind loads. Proceedings of the 4th European & African Conference on Wind Engineering EACWE 2005, Prague, Czech Republic, 11-15 July 2005.

[12] M. Matsumoto, H. Shirato, K. Araki, T. Haramura, T. Hashimoto. Spanwise coherence characteristics of surface pressure field on 2-D bluff bodies. *Journal of Wind Engineering and Industrial Aerodynamics*, **91**, 155-163, 2003.

[13] E.T. de Grenet, F. Ricciardelli. The span-wise correlation of aerodynamic forces on a rectangular cylinder for different vibration regimes. Proceedings of the 6th European Conference on Structural Dynamics EURODYN 2005, Paris, France, September 4-7, 2005.